# Modelling deformation and fracture of Gilsocarbon graphite subject to service environments

Savija, B.; Smith, Gillian E.; Heard, Peter J.; Sarakinou, Eleni; Darnbrough, James E.; Hallam, Keith R.; Schlangen, Erik; Flewitt, Peter E.J.

**DOI**
10.1016/j.jnucmat.2017.10.076

**Publication date**
2018

**Document Version**
Final published version

**Published in**
Journal of Nuclear Materials

Journal of Nuclear Materials 499 (2018) 18–28

Contents lists available at ScienceDirect

Journal of Nuclear Materials

journal homepage: www.elsevier.com/locate/jnucmat

# Modelling deformation and fracture of Gilsocarbon graphite subject to service environments

Branko Šavija [a, *], Gillian E. Smith [b], Peter J. Heard [b], Eleni Sarakinou [b], James E. Darnbrough [b], Keith R. Hallam [b], Erik Schlangen [a], Peter E.J. Flewitt [b, c]

[a] Microlab, Faculty of Civil Engineering and Geosciences, Delft University of Technology, Delft 22628 CN, The Netherlands
[b] Interface Analysis Centre, School of Physics, HH Wills Physics Laboratory, Tyndall Avenue, Bristol BS8 1TL, United Kingdom
[c] HH Wills Physics Laboratory, School of Physics, University of Bristol, Bristol BS8 1TL, UK

ARTICLE INFO

*Article history:*
Received 13 August 2017
Received in revised form
26 October 2017
Accepted 27 October 2017
Available online 8 November 2017

ABSTRACT

Commercial graphites are used for a wide range of applications. For example, Gilsocarbon graphite is used within the reactor core of advanced gas-cooled reactors (AGRs, UK) as a moderator. In service, the mechanical properties of the graphite are changed as a result of neutron irradiation induced defects and porosity arising from radiolytic oxidation. In this paper, we discuss measurements undertaken of mechanical properties at the micro-length-scale for virgin and irradiated graphite. These data provide the necessary inputs to an experimentally-informed model that predicts the deformation and fracture properties of Gilsocarbon graphite at the centimetre length-scale, which is commensurate with laboratory test specimen data. The model predictions provide an improved understanding of how the mechanical properties and fracture characteristics of this type of graphite change as a result of exposure to the reactor service environment.



## 1. Introduction

Unlike naturally occurring graphite, commercial graphites are used for a wide range of applications. However, in these cases the graphites usually have complex microstructures and are manufactured to have physical and mechanical properties appropriate to the specific application. An example of this is the Gilsocarbon graphite used in the construction of reactor cores for the civil power generating UK advanced gas-cooled reactors (AGRs), where properties have been achieved to allow the material to fulfil the structural and neutron moderation requirements. These bricks are a mixture of larger Gilsonite filler particles embedded in a matrix of filler particle flour mixed with pitch that has been moulded and graphitised as described previously [1]. Flaws and pores are introduced as a consequence of graphitisation. This produces complex interconnected nano- and micro-scale pathways that link many of the pores and flaws throughout the microstructure. In addition, changes arise from two processes: (i) neutron irradiation which introduces point defects into the crystal lattice; and (ii) radiolytic oxidation by the carbon dioxide gas as a result of gamma irradiation produced by nuclear fission. The latter causes graphite mass loss and a decrease in strength. The mechanical behaviour of these reactor core graphites can be described as quasi-brittle [1]. The materials have microstructural features similar to other aggregate-containing materials, such as concrete. Certainly, the nuclear graphite does not exhibit plasticity as it is deformed, so that non-linearity in the load displacement response is associated with micro-crack formation [1].

Of great importance for evaluating the integrity of graphite reactor cores is the evolution of bulk mechanical and physical properties over the service life. To understand this evolution for the AGR cores, regular measurements have been, and continue to be, made on macro-size samples removed periodically from reactors, either trepanned from bricks or extracted from surveillance schemes. However, these data do not separate contributions from irradiation damage and porosity induced by radiolytic oxidation to changes in the mechanical properties. In this respect, mechanical testing which uses micro-scale specimens is capable of targeting selected locations within the microstructure of a sample. Therefore,

* Corresponding author.
*E-mail addresses:* shavijabranko@yahoo.com (B. Šavija), gillian.e.smith@bristol.ac.uk (G.E. Smith), peter.heard@bristrol.ac.uk (P.J. Heard), eleni.sarakinou@bristol.ac.uk (E. Sarakinou), j.e.darnbrough@bristol.ac.uk (J.E. Darnbrough), k.r.hallam@bristol.ac.uk (K.R. Hallam), erik.schlangen@tudelft.nl (E. Schlangen), peter.flewitt@bristol.ac.uk (P.E.J. Flewitt).

https://doi.org/10.1016/j.jnucmat.2017.10.076

this approach provides a measure of the true properties of the solid regions of the graphite. Specifically, it is these data that are appropriate for input to microstructure-based models to predict the degradation of reactor core graphite over the service life. In this respect, a microstructurally-based, multi-length-scale finite beam element model is adopted to simulate the mechanical response and fracture characteristics of Gilsocarbon graphite in both the virgin and service-exposed conditions. For the latter, the focus is on simulating the combined contributions of mass loss by radiolytic oxidation and neutron irradiation damage on these properties.

## 2. Materials and experimental

Mechanical properties of virgin and irradiated Gilsocarbon graphite supplied by EDF Energy were measured. The polygranular Gilsocarbon graphite (IMI-Grade 21) material supplied is one of the nuclear-grade graphites used in the reactor cores of the AGR fleet of nuclear power stations in the UK. The fabrication route produces a relatively uniform distribution of filler particles in a graphitised matrix. In general, this material is considered to be macroscopically isotropic with respect to macroscale mechanical properties, with an elastic modulus of ~12 GPa, a tensile strength of ~20 MPa and a flexural strength of ~26 MPa in the virgin condition [2–5]. The overall microstructure comprises filler particles, binder phase and pores/flaws. Certainly, at the micro- and sub-micrometre length-scale pores and cracks arising from the fabrication process are distributed in the filler particles and matrix, and in this condition the total porosity is measured to be about 20% by volume. More details of the microstructure can be found elsewhere [2–8].

Mechanical property measurements were undertaken at the appropriate length-scale for input to numerical simulations. It is important to recognise that it is the inherent properties of the material, and not those of the overall microstructure, that are required. These include elastic modulus and fracture strength. For models used in this work, these data are required at the micrometre-scale. Micromechanical properties of this porous nuclear graphite were obtained using a technique for testing micro-cantilever specimens. For this, micro-scale cantilever beam specimens were tested within a combined focused ion beam and scanning electron workstation (FEI Helios NanoLab 600i) fitted with a customised force measurement system (Kleindiek Nanotechnik). The procedure is described in detail in other publications [2,10,12,15]. Two steps are required to produce an individual specimen. Step I is to gallium ion mill two rectangular slots 5 μm–15 μm apart depending on the size of the cantilevers to be made, with a 45° ion beam incident angle to the sample surface. For this step, an ion current of 6.5 nA was used. Step II repeats the milling at 45° from the other direction to form a square-sectioned cantilever beam, typically 5 μm × 5 μm x 10 μm or larger, depending on the required final size of the cantilever. Repeating the two steps with reduced ion beam currents of 2.7 nA and 0.9 nA, and invoking the 'cleaning cross-section' approach, produces a 2 μm × 2 μm x 10 μm cantilever beam (5:1 aspect ratio). The details of the loading system and calibration of the technique can be found elsewhere [2,10,12,15]. The force measurement system outputs the applied load (with a resolution of 0.01 μN) on the cantilever, whereas the displacement at the loading point is measured from the secondary electron microscopy images. More details about this experimental technique can be found in Refs. [2,9–12]. The irradiated sample provided had experienced a DIDO neutron dose equivalent of 93.1 × $10^{20}$n.cm$^{-2}$ (12.2 displacements per atom - dpa) and mass loss of 17.5%. These measurements on this length-scale were inputs for the multi-scale computer model.

## 3. Modelling approach

As described in Section 2, the Gilsocarbon graphite being considered consists of nearly-spherical filler particles and pores, with complex shapes embedded within the matrix. Microstructural models have been generated for virgin graphite (20% porosity) and to be representative of irradiated graphite (up to 60% porosity). Models of centimetre-sized cubes with 20% of the volume consisting of filler particles were created (Fig. 1), divided into eight 5 mm × 5 mm x 5 mm cubes, which were then subdivided into millimetre-sized cubes for the multi-scale fracture simulations. Details on the microstructural model creation, pore size and particle size distribution, and simulating the increase in porosity due to service conditions, are available elsewhere [13].

A lattice-type finite element model was used for the deformation and fracture analysis [13,14]. In this model, the material is discretised as a set of small beam elements. A regular cubic grid of beam elements, with equal lengths, is used. A set of linear analyses is then performed by calculating the response of the lattice mesh for a particular external displacement. The finite beam element with the highest stress-to-strength ratio is identified and removed from the lattice network. In each of the analysis steps, a single lattice beam element is removed from the mesh, representing the creation of a small crack, and causing a change in the specimen compliance. The analysis is then repeated, with an updated mesh.

To capture the microstructural details of porous graphite, the computational effort necessary for a single-scale approach is too high. To overcome this difficulty, in this study a multi-scale modelling scheme was used. The approach is shown schematically in Fig. 2. The multi-scale modelling procedure can be summarised as follows:

- First, the finite element beam microstructure is divided into a number of small cubes (in this case, each cube was 1 mm × 1 mm x 1 mm, with a total of 125 cubes).
- Then, a direct tension test is simulated on each of these small cubes (in these simulations, beam elements were assigned brittle behaviour), resulting in load-displacement curves, which are then represented as multi-linear (Fig. 2b).

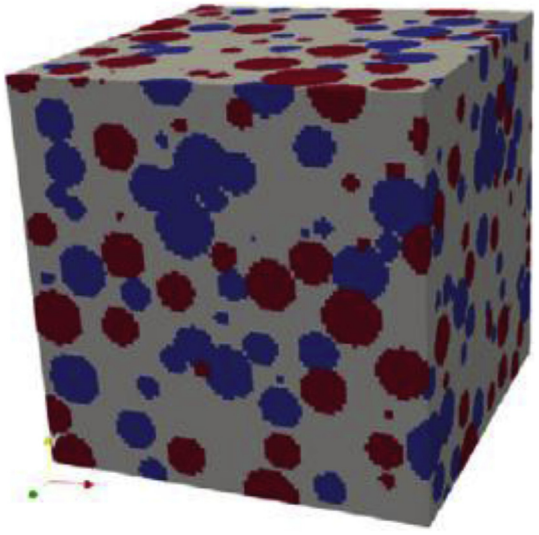

**Fig. 1.** Computer generated microstructure of Gilsocarbon graphite, with filler particles in red and large pores in blue (20%; 1 cm cube). Mass loss is simulated by 'removal' of matrix material to match the mass loss. (For interpretation of the references to colour in this figure legend, the reader is referred to the web version of this article.)

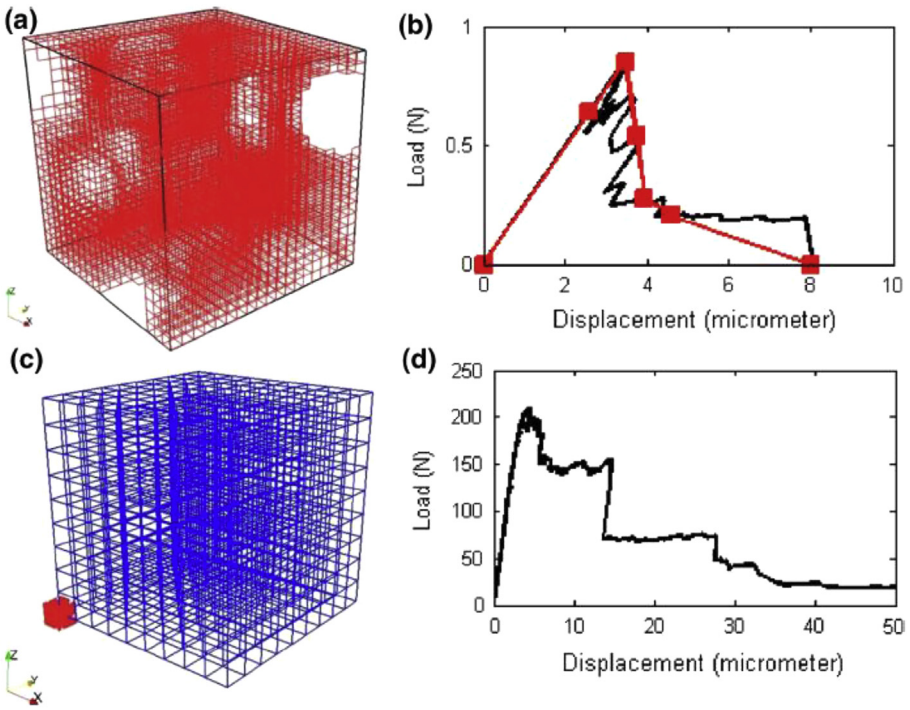


**Fig. 2.** Multi-scale modelling procedure: (a) a small cube, 20 × 20 x 20 voxels; (b) load-displacement curve (black), which is the outcome of a small-scale simulation. The grey curve is a schematisation of the black one and is multi linear, with six segments with points taken at (1) origin, (2) first micro-cracks, (3) peak load, (4) first point in response for which load is <75% of the peak, (5) first point in response for which load is <50% of the peak, (6) first point in response for which load is <25% of the peak, (7) point at which load is zero; (c) detailed mesh shows a small cube (20 × 20 x 20 voxels) in grey at its location within the large cube; (d) example load-displacement curve obtained from the full-scale simulation.

- These multi linear curves for small cubes are used as constitutive relationships for elements in the larger specimen (Fig. 2c), which is then tested, resulting in a load-displacement response and cracking patterns for the full-sized specimen (an example is shown in Fig. 2d).

In the simulations on the larger-scale, the local behaviour of each finite beam element was, therefore, not brittle. In fact, each element was assigned a multi-linear constitutive relationship that resulted in simulating the 'local' microstructure on the smaller-scale. Consequently, on this scale, the beam elements were not removed in each loading step but, for 'damaged' elements, the stiffness and strength were adjusted according to their respective constitutive relation.

## 4. Results and discussion

### 4.1. Mechanical properties

For the mechanical properties of the simulated graphite material, the values from micro-cantilever testing were used. The data measured at this length-scale are summarised in Table 1. It is noteworthy that these differ significantly from the bulk values given in Section 2 for virgin material. This is because the bulk data in Section 2 are measures of material with as-fabricated porosity and flaws. Moreover, since the micro-scale tests can provide data from selected microstructural features, we observe increases in both elastic modulus and flexural strength for the irradiated particles and a small decrease for the matrix compared with virgin material.

As input to the modelling, elastic moduli were used directly, while the uniaxial tensile strength of lattice beam elements were set to be 70% of the measured micro-cantilever bending strength. This was recommended in previous work by the authors [13]. For the unirradiated case, values measured on virgin Gilsocarbon graphite, as reported in Table 1, were used. For mass losses of 25% or more, values measured on the irradiated Gilsocarbon graphite, as reported in Table 1, were used. For the intermediate value of mass loss, 14.13%, a linear interpolation between the virgin and irradiated values was used.

Three-point bend geometry test specimens are adopted to undertake measurements of the mechanical properties of unirradiated and irradiated graphite samples as part of the reactor core monitoring scheme and supporting research programme. The mechanical property data available from these 6 mm × 6 mm x 15 mm specimens provide a basis for comparison with computer model predictions. As a consequence, in addition to undertaking modelling under tensile loading specific computer models were prepared and simulations produced for the three-point bend geometry specimens. Hence, model specimens of the same

**Table 1**
Summary of micro-cantilever test results.

| Condition | Measured area | Young's modulus (GPa) | Bending strength (MPa) | Tensile strength in model (70% of bending strength) (MPa) |
|---|---|---|---|---|
| Unirradiated | Filler particle and matrix [9] | 18 | 564 | 395 |
| Irradiated | Filler particle | 24 | 1093 | 760 |
| | Matrix | 14 | 330 | 231 |

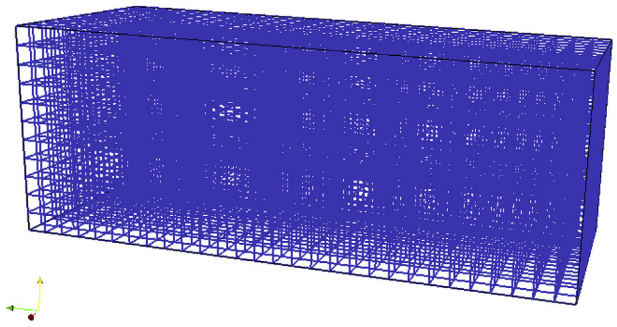

**Fig. 3.** Specimen used in three-point bending simulation.

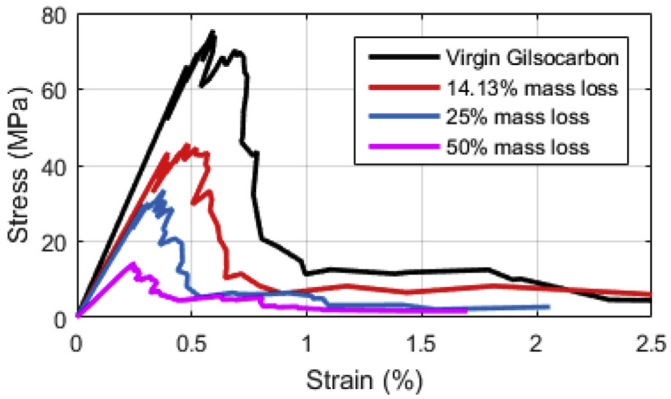


**Fig. 5.** Simulated stress strain curves for Gilsocarbon graphite with increasing levels of irradiation damage (legend denotes mass loss).

dimensions as those used in experiments were simulated using a lattice mesh of 12 nodes × 12 nodes x 30 nodes (Fig. 3). Loading was applied in the middle and the beam was simply supported. Each beam in the lattice was randomly assigned with a multi-linear curve coming from small cubes of the corresponding mass loss case. Note that since the mechanical properties were randomly distributed and do not exactly follow the material microstructure, as was the case for uniaxial tension, this could lead to somewhat different strengths. To compensate for this effect, the random assignment procedure was repeated five times for each mass loss case, and five specimens were simulated in each case.

### 4.2. Modelling

To implement the computer modelling, porosity levels were converted to mass loss values, and the change of engineering properties (elastic modulus and strength) caused by combined contributions of radiolytic oxidation and neutron irradiation may be predicted. A benefit of the multi-scale modelling procedure is that it enables a statistical evaluation of strength distributions in the sub-microstructures. This analysis provides a measure of the variability of strengths in the model graphite material. Histograms of simulated uniaxial strengths for increasing porosity levels are given in Fig. 4. They show a shift towards the left with increasing mass loss, signifying weakening of the material. In addition, there is a progressive decrease in the width of the distributions (full width half maximum), indicating that scatter is reduced as the amount of irradiation-induced porosity increases.

In Fig. 5, simulated tensile stress/strain curves for the unirradiated material and three mass loss levels are given, where zero represents the unirradiated condition that contains porosity arising solely from fabrication. It is evident that for the increasing levels of neutron irradiation combined with mass loss there is a progressive decrease in the predicted elastic modulus and tensile strength. This is seen in the comparison between measured and simulated elastic moduli for increasing mass loss given in Fig. 6. Note that experiments were performed on 6 mm × 6 mm x 15 mm specimens

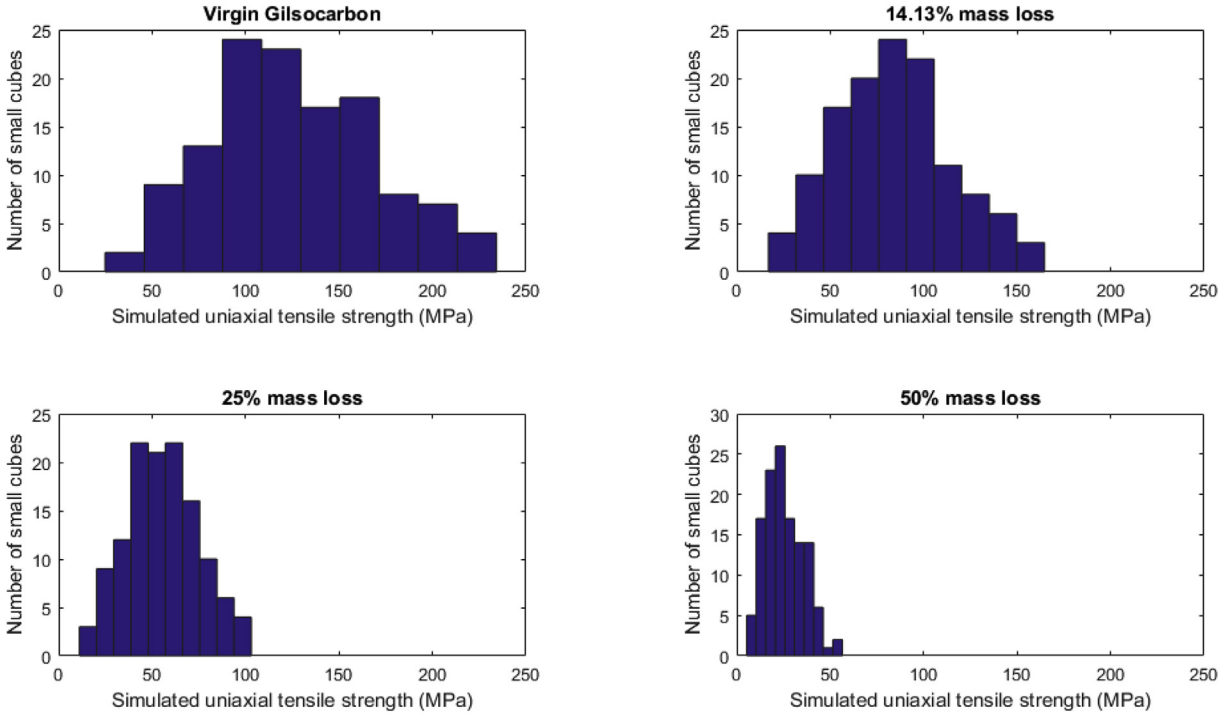


**Fig. 4.** (a)–(d) Distribution of uniaxial strengths of small (1 mm × 1 mm x 1 mm) cubes in microstructures with increasing levels of mass loss, up to 50%. (Vertical scale in (d) is from zero to 30%.).

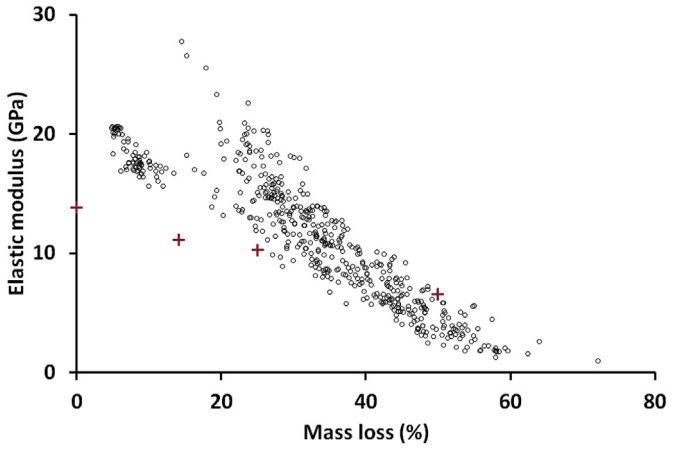


**Fig. 6.** Comparison of simulated (cross) and experimental (circle) values of elastic modulus for increasing mass loss.

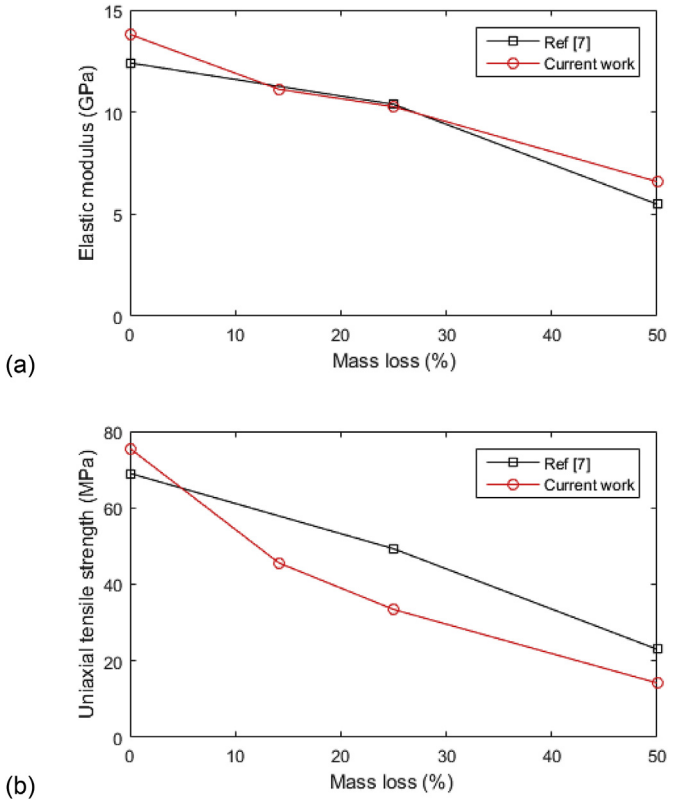


**Fig. 7.** Comparison of (a) simulated elastic moduli and (b) uniaxial tensile strength from previous work [3] (not considering neutron irradiation effects) and current work. Note that strength values from Ref. [3] were scaled by 0.7 to enable the comparison.

tested in three-point bending. In this case, the predicted values follow the experimentally-measured trend of modulus decrease with increasing mass loss. In Fig. 6, there is a very good fit between the values of elastic modulus predicted by the computer modelling and experimental data assembled from in-service trepanned sample measurements and a research programme undertaken in a test reactor. It is well established that changes in mechanical properties of nuclear graphite depend upon the level of neutron irradiation [16]. In general, the early stages of exposure produce behaviour that is dominated by irradiation strengthening, which potentially leads to increases in both strength and elastic modulus. However, prolonged exposure radiolytic oxidation will cause further mass loss which will become a dominating factor and lead to a reduction in mechanical performance [17].

In previous work [13], changes in properties for the same Gilsocarbon graphite model material with increasing mass loss, but without considering neutron irradiation, were simulated. The same computer-generated microstructures were used as input for the numerical model, as in the current work. The comparison between the two scenarios is given in Fig. 7. In this sensitivity analysis, for the elastic modulus there is no significant difference when considering or not the irradiation effect. In terms of tensile strength, however, there is a significant difference. Neglecting the effect of neutron irradiation, which, according to micro-cantilever testing, hardens the filler particles but significantly reduces the strength of the matrix (see Table 1), is not conservative and leads to overestimation of tensile strength. This can, in practice, lead to an underestimation of the risk of cracking in reactor core bricks. It is, therefore, important to continue research on changes of (micro-) mechanical properties of nuclear graphite with neutron irradiation. The predicted evolution of cracks occurring in uniaxial tension simulations is given in Figs. 8–9. In the virgin Gilsocarbon material (Fig. 8), the cracks start in the matrix, where porosity is located. It is noteworthy that experimental observations show the mass loss to be concentrated in the matrix. However, cracking then propagates through the filler particles and forms a single crack plane. This is a result of three assumptions in the present model: (1) mechanical properties of the matrix and the filler particles are the same in the unirradiated condition; (2) the interface between the filler particle and the graphite matrix has the same mechanical properties as the filler particle; and (3) the existence of micro-cracks in the filler particles (i.e. both transverse cracks and 'onion ring' flaws) has been neglected in the present simulations for simplicity. With increasing irradiation, it is clear that cracking localises in the matrix phase, completely avoiding the particles. This is because, according to micro-cantilever measurements, the filler particles become stronger and stiffer with neutron irradiation while the matrix phase becomes softer and weaker. It is seen that with increasing porosity the width of the fracture process zone increases. This trend has also been observed in other porous materials, such as concrete [18] and gypsum plaster [14]. The increase in porosity also marks a transition from relatively brittle to more quasi-brittle behaviour, evident also in stress/strain curves (Fig. 5).

Quasi-brittle fracture is typically characterised by three distinct regions in the load-displacement curve for a quasi-brittle material, such as nuclear graphite (shown schematically in Fig. 10) [19,20]: the linear-elastic region (Region I); the micro-cracking region (Region II), which occurs prior to the peak load; and the post-peak region (Region III), in which softening of the material is observed. As stated previously, nuclear graphite does not show a significant ability for plastic deformation. Therefore, changes in compliance are a result of (micro-)cracking. Different regions in the stress/strain curve are characterised by the energy needed for fracture. For uniaxial tension simulations presented in this report, energy required for fracture is calculated using Equation (1) and given in Table 2.

$$G_f = \int_0^{u_1} \sigma du \tag{1}$$

where $\sigma$ is the stress and $u$ the corresponding displacement. From

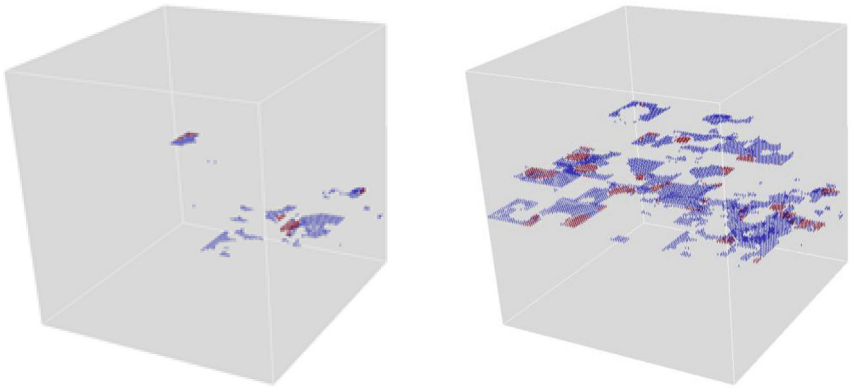

**Fig. 8.** Cracks formed in a simulated uniaxial tensile test of a virgin Gilsocarbon specimen. Left - at peak load; Right - at failure. Blue - matrix; Red - filler particle; White - particle/matrix interface. Loading was applied in the vertical direction. (For interpretation of the references to colour in this figure legend, the reader is referred to the web version of this article.)

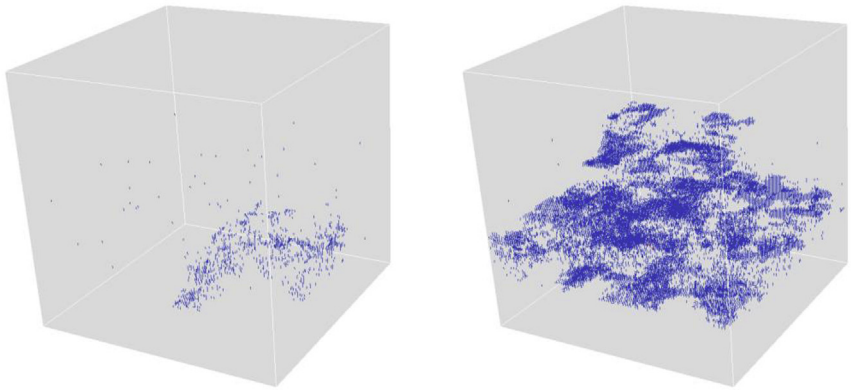

**Fig. 9.** Cracks formed in a simulated uniaxial tensile test of an irradiated Gilsocarbon specimen with 50% mass loss. Left - at peak load; Right - at failure. Blue - matrix; Red - filler particle; White - particle/matrix interface. Loading was applied in the vertical direction. (For interpretation of the references to colour in this figure legend, the reader is referred to the web version of this article.)

Table 2, it can be seen that the percentage of the total energy of fracture consumed after the peak load is significantly higher after neutron irradiation and radiolytic oxidation compared to the virgin Gilsocarbon case. It can be stated that the graphites exposed to in-service conditions are tougher than the virgin graphite, and this could potentially be an important factor when assessing the residual service life of a plant.

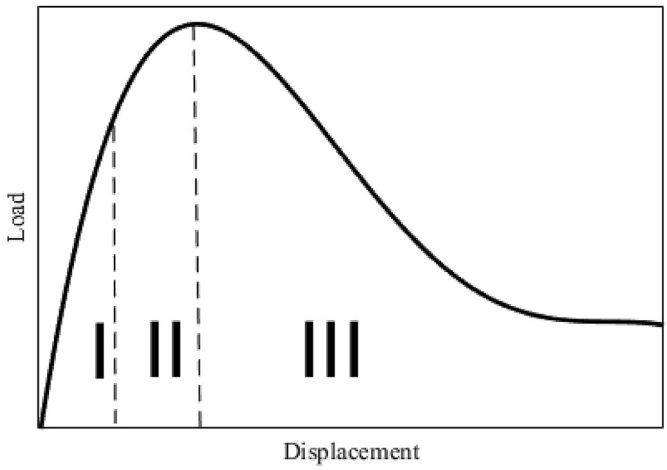


**Fig. 10.** Schematic load-displacement curve for a quasi-brittle material: Region I - linear; Region II - non-linear; Region III - post-peak softening.

Since all experimental measurements were performed using three-point bending geometries, and not uniaxial tension, additional (simplified) simulations of three-point bending were performed, as described. Stress/displacement curves of simulated three-point bending tests for all cases are shown in Fig. 11. Five different realisations of the model were simulated for each condition. All results are also given in Table 3. It is seen that variation exists between individual model predictions for each condition. Also, the standard deviation decreases as the mass loss (i.e. porosity) increases. However, when normalised to the mean the percentage deviation remains constant. In our previous work with model quasi-brittle materials [14] it was shown that the variation in simulated flexural strength between individual model realisations decreases as the (controlled) porosity increases. This is of practical significance because graphite specimens tested in the laboratory are significantly smaller than the reactor core bricks, and it was shown that the variability between individual test results is higher for smaller specimen size [13]. Consequently, a large number of laboratory specimens need to be tested to obtain results that can be reliably used for practical purposes. However, based on the results of this and previous work [14], it is probable that for graphite bricks

**Table 2**
Simulated fracture energy ($G_f$) in uniaxial tension simulations.

| Condition | Fracture energy consumed in the elastic regime (N.mm) | Fracture energy consumed in the inelastic regime (up to peak load) (N.mm) | Relative fracture energy consumed before peak load (%) | Fracture energy consumed in the inelastic regime (after peak load) (N.mm) | Relative fracture energy consumed after peak load (%) | Total fracture energy (N.mm) |
|---|---|---|---|---|---|---|
| Virgin | 0.648 | 0.184 | 24.13 | 2.617 | 75.88 | 3.449 |
| 14.13% mass loss | 0.013 | 0.168 | 10.73 | 1.506 | 89.27 | 1.687 |
| 25% mass loss | 0.013 | 0.092 | 16.85 | 0.520 | 83.15 | 0.623 |
| 50% mass loss | 0.0002 | 0.017 | 5.89 | 0.275 | 94.11 | 0.292 |

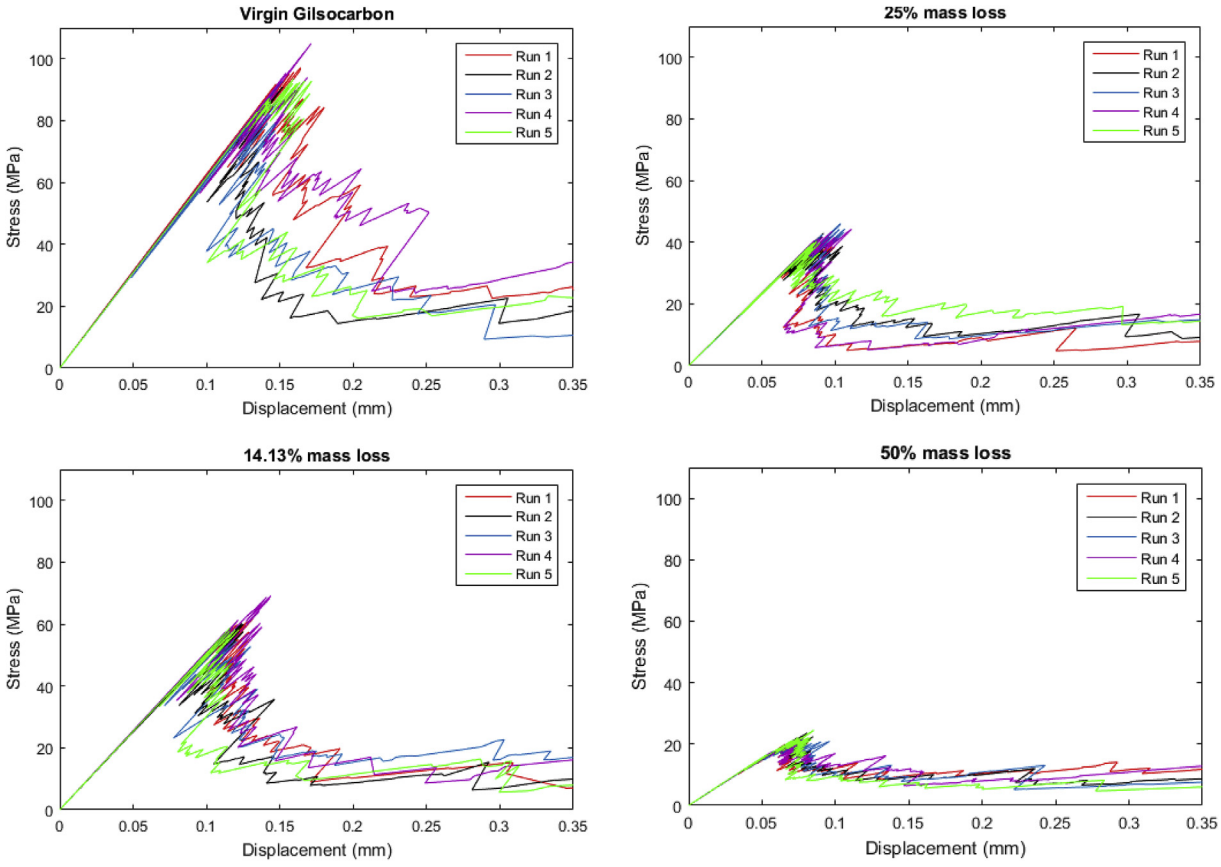


**Fig. 11.** Simulated stress/displacement diagrams for three-point bending specimens with varying mass loss (five random simulations per case).

**Table 3**
Summary of three-point bending strengths obtained from models, as shown in Figs. 14–15.

| Condition | Bending strength (MPa) | | | | | | |
|---|---|---|---|---|---|---|---|
| | Run1 | Run2 | Run3 | Run4 | Run5 | Mean | Standard deviation |
| Virgin | 97.12 | 90.98 | 93.09 | 104.85 | 93.43 | 95.90 | 4.89 |
| 14.13% mass loss | 61.78 | 60.17 | 55.40 | 69.14 | 58.78 | 61.06 | 4.55 |
| 25% mass loss | 40.34 | 42.94 | 46.07 | 44.24 | 40.39 | 42.80 | 2.22 |
| 50% mass loss | 20.91 | 23.54 | 21.55 | 21.88 | 24.44 | 22.46 | 1.32 |

exposed to service conditions a smaller number of specimens needs to be tested.

Simplified three-point bending simulations show, in general, that the material exhibits quasi-brittle behaviour for all simulated cases. Similar to uniaxial tension simulations, the post-peak behaviour becomes more pronounced with increasing mass loss (i.e. porosity). Again, decreasing bending strength with increasing mass loss is observed, in accordance with simulated uniaxial tension experiments. In Fig. 12, a comparison is given between results of the simplified statistical model and experimental measurements. Considering the very limited number of input parameters needed for the present model and the underlying assumptions in the small-

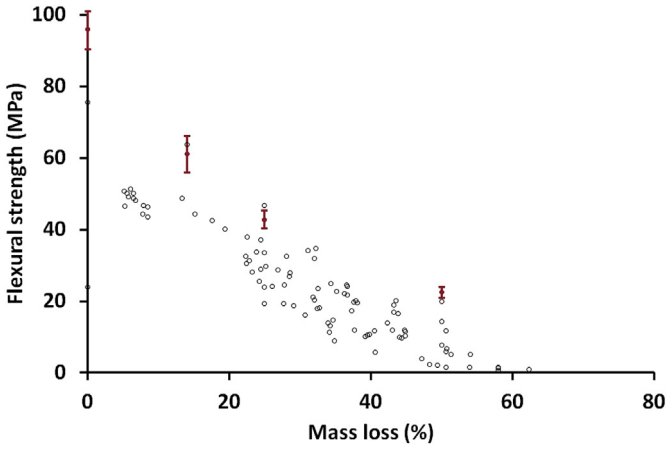


**Fig. 12.** Comparison of simulated (filled circle) and experimental (open circle) values of flexural strength for increasing mass loss. Error bars indicate standard deviation between five simulations.

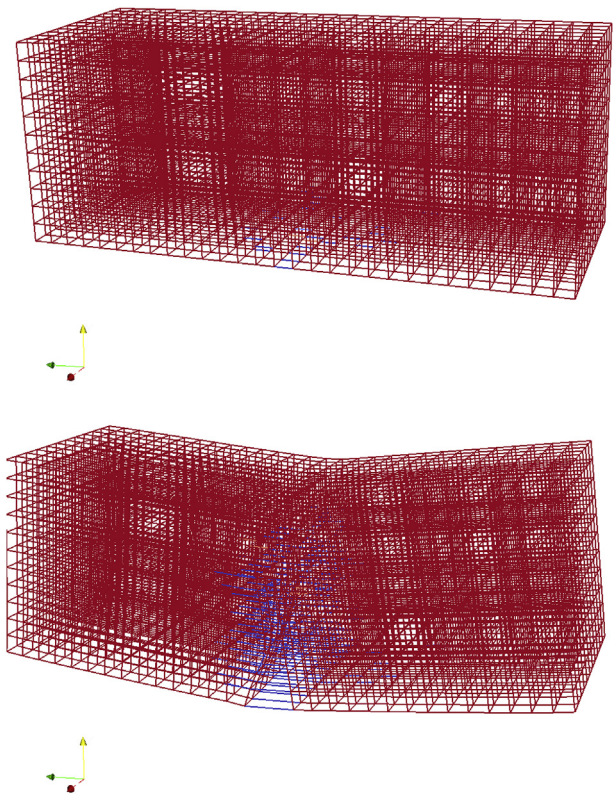

**Fig. 13.** Undeformed mesh (top) and deformed mesh (bottom) of a simulated virgin Gilsocarbon specimen subjected to three-point bending. Damaged elements are shown in blue. (For interpretation of the references to colour in this figure legend, the reader is referred to the web version of this article.)

scale modelling, an excellent fit is observed between experiments and simulations for in-service conditions. Simulated flexural strengths are slightly higher than experimental values, but this can most probably be improved by a more rigorous description of the material microstructure and taking into account features such as onion ring porosity in the filler particles [11]. Furthermore, since only one realisation of the material microstructure was simulated (Fig. 1), it may be of use to also consider this in a statistical way.

In Fig. 13, a deformed mesh for one of the simulations is given. Here it can be seen that, in general, failure is caused by macro-crack propagation through the middle of the specimen. This is expected for a quasi-brittle material. More information can be obtained from the damage evolution. In Figs. 14 and 15, damage evolution for two extreme mass loss levels (i.e. 0% and 50%) is presented, together with corresponding pattern of crack distribution. Note that damage states shown correspond to different element states as defined by multi-linear constitutive relationships of each individual element (e.g. as shown in Fig. 2d). Therefore, element states go from undamaged to completely broken following the multi-linear curve of each element. Essentially, elements that are damaged but not completely cracked reveal significantly different extents of micro-cracking. While it is clear that, in both cases, a single (macro-)crack localises, the damage zone becomes wider with increasing mass loss. This also corresponds very well with the simulated uniaxial tension experiments, where the fracture process zone becomes wider as the mass loss (i.e. porosity) increases. The present simplified model used for simulating three-point bending experiments is able, therefore, to reproduce the major features of the detailed microstructurally-based model (as used for simulating uniaxial tension), i.e the quasi-brittle behaviour, the change in (measured) mechanical properties with changing porosity and irradiation conditions, and the widening of the damage zone with increasing mass loss. When simulating larger specimens and moving towards full-scale brick elements, there is a clear benefit of reduced computational time. On the other hand, the level of detail obtained from such a simulation is lower compared to the microstructural model. Furthermore, it cannot provide mechanistic understanding of the fracture process in a multi-phase material such as Gilsocarbon graphite. The microstructural model can show which phase is critical for initiation and propagation of cracking. Since the long-term goal of the modelling efforts presented here is to evaluate remaining service life predictions, a compromise between the two approaches may suffice. A detailed approach would focus on the understanding of the process and sensitivity analyses, while the simplified approach could be used for engineering purposes. A similar statistical approach was recently proposed [21]. If a database of (simulated) material properties was available from the microstructural approach, statistical analyses could then be performed on the larger-scale. This approach would then be upscaled all the way to component length-scale, where statistical finite element modelling would then be applied. Note that full-scale modelling would also require knowledge of material gradients inside individual components, e.g. different exposures of the inner and outer layers in individual reactor core bricks resulting in mass loss/irradiation state gradients, which could be accommodated by the proposed approach.

## 5. Concluding comments

In Section 5, we have described and discussed results of a multi-scale model used for predicting changes in elastic properties of Gilsocarbon graphite due to service exposure to combined neutron irradiation and radiolytic oxidation. The model is founded on two underlying assumptions: (1) a good description of the material microstructure is necessary; and (2) material properties measured at the appropriate length-scale are needed to describe the deformation and fracture process in a complex multi-phase material

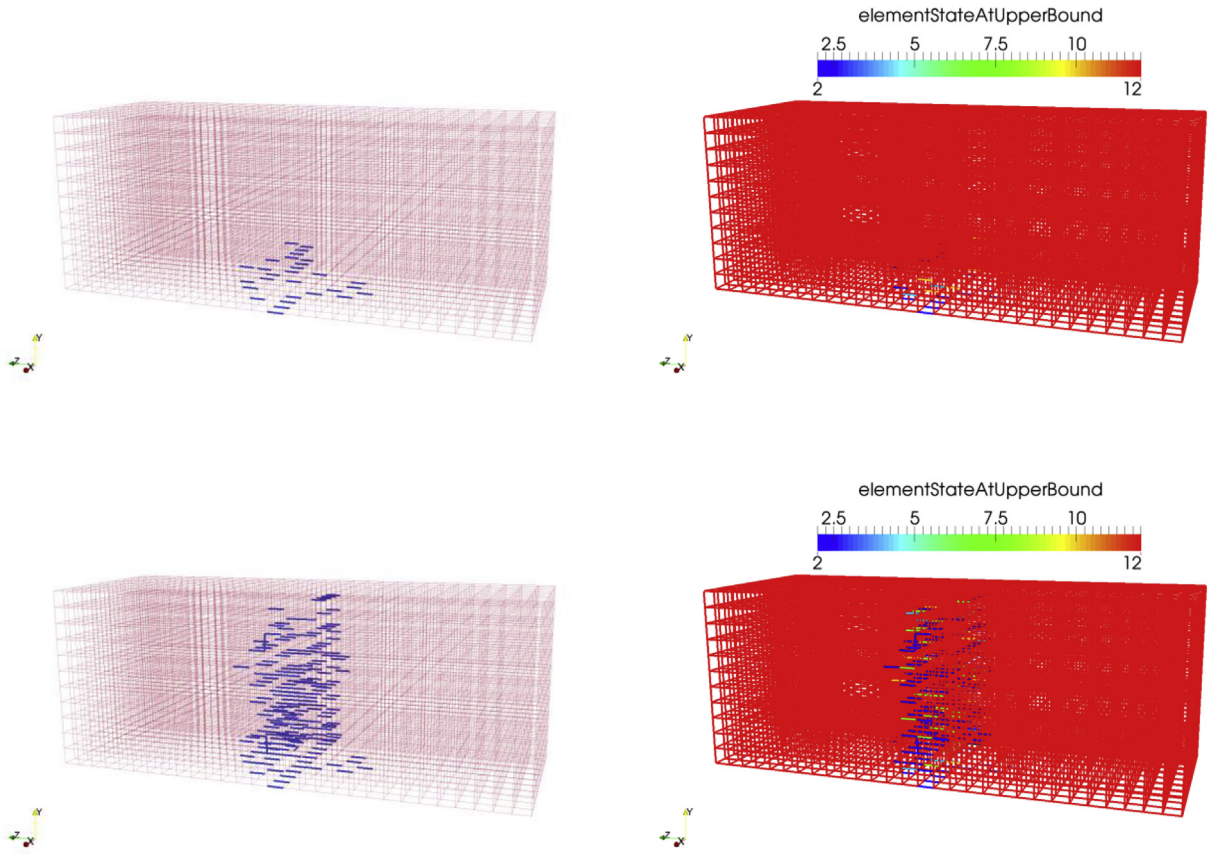


**Fig. 14.** Damage development in virgin Gilsocarbon specimen subjected to three-point bending. Left - cracks only; Right - damaged elements according to corresponding multi-linear damage law as given, for example, in Fig. 2b. Here, elementStateAtUpperBound 12 (red) signifies an intact beam element, while 2 (blue) signifies a completely damaged element. (For interpretation of the references to colour in this figure legend, the reader is referred to the web version of this article.)

such as Gilsocarbon graphite. The model is informed by experimental measurements of 'true' material properties. In this work, mechanical properties (elastic modulus and fracture strength) of virgin and irradiated Gilsocarbon graphite are obtained using a micro-cantilever testing technique. By testing micrometre length-scale specimens, this technique enables material properties of specific features of the microstructure to be obtained via minimisation of the influence of porosity and defects on the measurement results. This is essential for multi-phase materials that exhibit heterogeneities and porosities at multiple length-scales, such as nuclear graphite [9] and cement paste [22–25]. These measurements provide the necessary input data at the micro-length-scale. In addition, a microstructural model representative of the Gilsocarbon graphite and the changes affecting it over time has been invoked. Therefore, porosity is explicitly included in the microstructural model. This procedure avoids the need for fitting parameters, so the simulation results are fully predictive and dependent on a good microstructural model. This makes data collection and property prediction cheap and efficient.

Two different approaches, with varying levels of detail, have been presented: (1) a fully microstructural approach, which has been used to simulate uniaxial tension experiments on the millimetre length-scale; and (2) a statistical microstructure-informed approach, which has been used to simulate three-point bending experiments at the centimetre length-scale, with size corresponding to experiments. Simulation results have been compared to experimental data. Uniaxial tension simulations have shown excellent agreement between simulated elastic moduli and those measured for various in-service conditions. In addition, simulations have shown a shift between relatively brittle to more quasi-brittle behaviour with increasing irradiation and mass loss, signified by an increased contribution of the post-peak work of fracture, accompanied by widening of the fracture process zone. The crack propagation mode changes with increasing irradiation due to strengthening of the filler particles. While virgin condition cracks do penetrate through the filler particles, following irradiation this is not the case. For three-point bending simulations, a simplified statistical microscale approach has been adopted. While this does not explicitly use the material microstructure as input, it is informed by smaller-scale simulations. In a statistical way, this makes the proposed approach significantly less computationally expensive and, therefore, more suitable for larger specimens. Simulation results have shown good agreement with experimental data in terms of flexural strength. Although simplified, this approach is able to reproduce the main behaviours of the more detailed microstructurally-based approach (such as widening of the damage zone with increasing porosity), but with less detail.

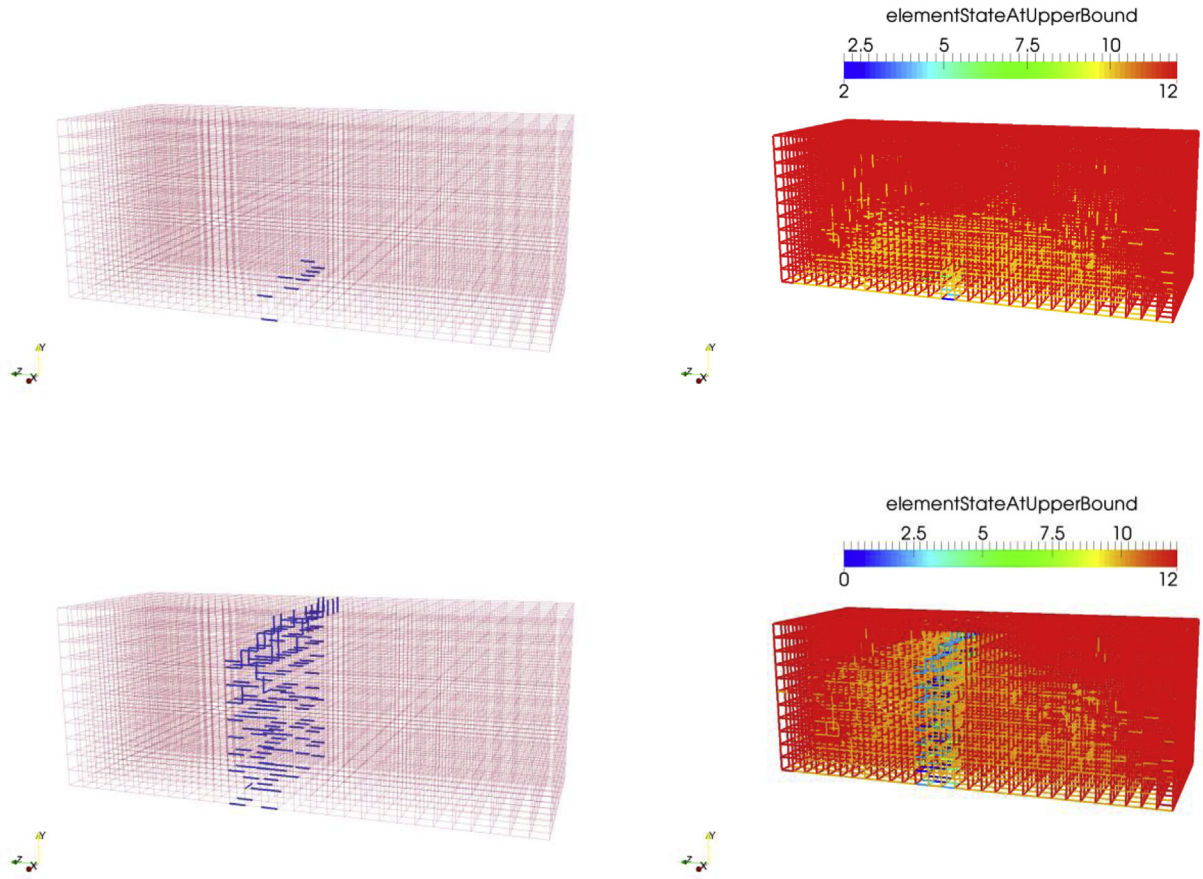


**Fig. 15.** Damage development in irradiated Gilsocarbon specimen with 50% mass loss subjected to three-point bending. Left - cracks only; Right - damaged elements according to corresponding multi-linear damage law as given, for example, in Fig. 2b. Here, elementStateAtUpperBound 12 (red) signifies an intact beam element, while 2 (blue) signifies a completely damaged element. (For interpretation of the references to colour in this figure legend, the reader is referred to the web version of this article.)

## Funding sources

This work was supported by the Engineering and Physical Sciences Research Council (grant number EP/M018598/1) and EDF Energy.

## Acknowledgements

The authors acknowledge support by EDF Energy Limited. The paper is published with the permission of Dr J Reed, EDF Energy Limited. The views expressed are those of the authors.

## Appendix A. Supplementary data

Supplementary data related to this article can be found at https://doi.org/10.1016/j.jnucmat.2017.10.076.

## References

[1] R. Moskovic, P.E.J. Flewitt, E. Schlangen, G.E. Smith, A.G. Crocker, A. Hodgkins, P.J. Heard, M.R. Wootton, Understanding fracture behaviour of PGA reactor core graphite: perspective, Mater. Sci. Technol. 30 (2014) 129–145.
[2] D. Liu, P.J. Heard, S. Nakhodchi, P.E.J. Flewitt, Small-scale approaches to evaluate the mechanical properties of quasi-brittle reactor core graphite, in: N. Tzelepi, M.C. Carroll (Eds.), Graphite Testing for Nuclear Applications: the Significance of Test Specimen Volume and Geometry and the Statistical Significance of Test Specimen Population, 2014, pp. 84–104. ASTM International STP157820130127.
[3] P.J. Heard, M.R. Wooton, R. Moskovic, P.E.J. Flewitt, Crack initiation and propagation in pile grade A (PGA) reactor core graphite under a range of loading conditions, J. Nucl. Mater. 401 (2010) 71–77.
[4] T.J. Marrow, D. Liu, S.M. Barhli, L. Saucedo Mora, Y. Vertyagina, D.M. Collins, C. Reinhard, S. Kabra, P.E.J. Flewitt, D.J. Smith, In situ measurement of the strains within a mechanically loaded polygranular graphite, Carbon 96 (2016) 285–302.
[5] J.E. Brocklehurst, M.I. Darby, Concerning the fracture of graphite under different test conditions, Mater. Sci. Eng. A 16 (1974) 91–106.
[6] J. Mileeva, D.K. Ross, S.M. King, A study of the porosity of nuclear graphite using small-angle neutron scattering, Carbon 64 (2013) 20–26.
[7] Y. Vertyagina, T.J. Marrow, Multifractal-based assessment of Gilsocarbon graphite microstructures, Carbon 109 (2016) 711–718.
[8] G.M. Laudone, C.M. Gribble, G.P. Matthews, Characterisation of the porous structure of Gilsocarbon graphite using pycnometry, cyclic porosimetry and void-network modelling, Carbon 73 (2014) 61–70.
[9] D. Liu, P.E.J. Flewitt, Deformation and fracture of carbonaceous materials using in situ micro-mechanical testing, Carbon 114 (2017) 261–274.
[10] J.E. Darnbrough, D. Liu, P.E.J. Flewitt, Microscale testing of ductile and brittle cantilever beam specimens in situ with a dual beam workstation, Meas. Sci. Technol. 24 (2013) 055010.
[11] D. Liu, P.J. Heard, P.E.J. Flewitt, Microscale testing to evaluate the fracture characteristics of quasi-brittle material, in: Proceedings of the 13th International Conference on Fracture, Beijing China, 2013.
[12] D. Liu, P.J. Heard, P.E.J. Flewitt, D.J. Smith, Challenges associated with measuring the mechanical properties of reactor core graphites for input to durability models, in: P.E.J. Flewitt, A.J. Wickham (Eds.), The 4th EDF Energy Nuclear Graphite Symposium: Engineering Challenges Associated with the Life of Graphite Reactor Cores, EMAS, Warrington, UK, 2014, pp. 413–426.
[13] B. Šavija, D. Liu, G.E. Smith, K.R. Hallam, E. Schlangen, P.E.J. Flewitt, Experimentally informed multi-scale modelling of mechanical properties of quasi-brittle nuclear graphite, Eng. Fract. Mech. 153 (2016) 360–377.
[14] D. Liu, B. Šavija, G.E. Smith, P.E.J. Flewitt, T. Lowe, E. Schlangen, Towards understanding the influence of porosity on mechanical and fracture behaviour of quasi-brittle materials: experiments and modelling, Int. J. Fract. 205 (2017) 57–72.
[15] D. Liu, P.E.J. Flewitt, The measurement of mechanical properties of thermal barrier coatings by micro-cantilever tests, Key Eng. Mater. 525–526 (2013) 13–16.
[16] T.D. Burchell, Radiation Effects in Graphite, Oak Ridge National Laboratory,

2012.
[17] J.D. Lord, N.J. McCormick, J. Urquhart, G.M. Klimaytys, I.J. Lingham, Measuring the static modulus of nuclear graphite from four-point flexural strength tests and DIC, Appl. Mech. Mater. 24–25 (2010) 385–390.
[18] K. Haidar, G. Pijaudier-Cabot, J.-F. Dubé, A. Loukili, Correlation between the internal length, the fracture process zone and size effect in model materials, Mater. Struct. 38 (2005) 201–210.
[19] J.G.M. Van Mier, Concrete fracture: a Multiscale Approach, CRC Press, 2012.
[20] S.P. Shah, S.E. Swartz, C. Ouyang, Fracture Mechanics of Concrete: Applications of Fracture Mechanics to Concrete, Rock and Other Quasi-brittle Materials, John Wiley and Sons, 1995.
[21] M. Bansal, I.V. Singh, B.K. Mishra, K. Sharma, I.A. Khan, A numerical prediction of flexural strength probability for NBG-18 nuclear grade graphite using strength pair model, J. Strain Analysis Eng. Des. 52 (3) (2017) 204–211, 0309324717698609.
[22] J. Němeček, V. Králík, V. Šmilauer, L. Polívka, A. Jäger, Tensile strength of hydrated cement paste phases assessed by micro-bending tests and nano-indentation, Cem. Concr. Compos. 73 (2016) 164–173.
[23] H. Zhang, B. Šavija, S. Chaves Figueiredo, M. Lukovic, E. Schlangen, Microscale testing and modelling of cement paste as basis for multi-scale modelling, Materials 9 (2016) 907.
[24] B. Šavija, H. Zhang, E. Schlangen, Influence of microencapsulated phase change material (PCM) addition on (micro) mechanical properties of cement paste, Materials 10 (8) (2017) 863.
[25] H. Zhang, B. Šavija, S. Chaves Figueiredo, E. Schlangen, Experimentally validated multi-scale modelling scheme of deformation and fracture of cement paste, Cem. Concr. Res. 102 (2017) 175–186. https://doi.org/10.1016/j.cemconres.2017.09.011.